1918
TALLINNA TEHNIKAÜLIKOOL
TALLINN UNIVERSITY OF TECHNOLOGY
Institute of Electronics

Modelling of terahertz broadband radiation sources based on GaAs/AlGaAs quantum well heterostructures

Kvantaukudega GaAs/AlGaAs heterostruktuuridel põhinevate laiaribaliste terahertskiirgurite modelleerimine

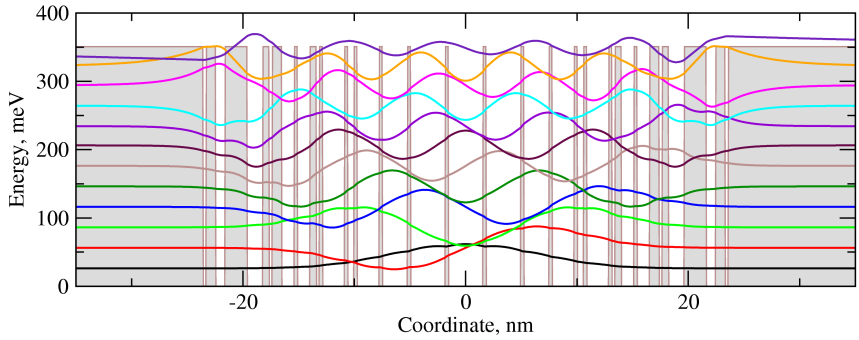

Master Thesis

Reeno Reeder

Supervisor: Andres Udal, PhD
senior researcher

Tallinn 2007

Abstract

This work handles the field of semiconductor quantum electronics and is based mainly on tasks to solve Schrödinger equation and to model electron transport in GaAs/AlGaAs multibarrier heterostructures. The work contains two major parts.

The first part of the work stands for finding proper numerical method to solve 1D time-independent Schrödinger equation. It was found that the best way is to use standard linear algebra solvers for eigenvalue problem. There are 3 papers published on this topic.

The second part covers the methodology of calculating the emission characteristics for laterally pumped quantum well heterostructures based emitters. The effect of lateral electric field is explored and relevant methods presented. Calculations are done for digitally graded parabolic quantum wells and results are presented in a separate manuscript. There are 2 papers waiting for acceptance on this topic.

The results show that a real emitter can be built using only one layer. For 7 THz emitter the overall emitted power rises higher than black body radiation.

The work is written in English, it contains 4 chapters, 3 tables and 10 figures on 25 pages. The work has 5 scientific papers in the appendix.

Key words: Schrödinger equation, shifted Fermi-Dirac distribution function, digitised parabolic quantum well, lateral transport, terahertz emitter

Resümee

Töö käsitleb pooljuht-kvantelektroonika valdkonda ja baseerub peamiselt Schrödingeri võrrandi lahendamisele ja elektroni transpordi modelleerimisele GaAs/AlGaAs multibarjääridega heterostruktuurides. Töö koosneb kahest peamisest osast.

Esimene töö osa puudutab sobivaima numbrilise meetodi leidmist ühemõõtmelise ajast sõltumatu Schrödingeri võrrandi lahendamiseks. Parimaks viisiks osutus standardne lineaaralgebra lahendusmeetod omaväärtusprobleemi jaoks. Sellel teemal on publitseeritud 3 teaduslikku artiklit.

Teine osa käsitleb lateraalselt ergastatud kvantauk-heterostruktuuridel baseeruvate kiirgurite emissioonikarakteristikute arvutamismetoodikat. Uuritakse lateraalse elektrivälja mõju ja tutvustatakse seonduvaid meetodeid. Arvutused on tehtud digitaalselt tasandatud paraboolsete kvantaukude jaoks ja tulemused on esitatud eraldi käsikirjas. Sellel teemal on avaldamise ootel 2 teaduslikku artiklit.

Tulemused näitavad, et ühel kihil baseeruvat emitterit on reaalselt võimalik ehitada. 7 THz kiirguri jaoks ületab kiiratav võimsus musta keha kiirgusvõimsuse.

Töö on kirjutatud inglise keeles, see koosneb 4 peatükist, 3 tabelist ja 10 joonisest 25 leheküljel. Tööl on lisana 5 artiklit.

Võtmesõnad: Schrödingeri võrrand, nihutatud Fermi-Diraci jaotusfunktsioon, digitaliseeritud paraboolne kvantauk, lateraalne transport, terahertskiirgur

Acknowledgements

My special thanks go to Prof. Paul Harrison who inspired me to work in this field and who gave me the opportunity to work in Leeds University for 4 months. I thank Zoran Ikonic for valuable advices and fruitful supervision during my work period in Leeds. I would like to thank all the quantum electronics group members from room 255 in Leeds University, who ensured great social environment for doing this research (Leon Lever, Alex Valavanis, Nenad Vukmirović, etc).

I would like to express gratitude to my supervisor Andres Udal who has put a lot of effort to guide me during my Master studies. He was also the supervisor of my Bachelor thesis. I thank also Professor Enn Velmre who helped me to understand the theoretical problems in this field.

I thank my employer Cybernetica AS for giving me flexible work conditions, so that I could do my studies. I would also like to thank Estonian Archimedes Foundation for funding my studies at Leeds University and Estonian Science Foundation for supporting this work by grants 5911 and 6914.

Contents

Chapter 1

Introduction

The development of sources of terahertz radiation has become hot topic in the last decade because of numerous prospective applications in spectroscopy, imaging and communications [1]. The major application of terahertz radiation is related to spectroscopy, as all the chemical elements have a unique "frequency label" at terahertz region. Sensing of chemical elements, monitoring pollution, and detection of noxious substances are some examples of such applications. Spectroscopy is therefore a sphere that needs the most the advantages of terahertz emission.

Today, most of the coherent terahertz sources need to work at very low temperatures, which makes them expensive to use. Fortunately not all the applications need the coherent radiation, they can work with incoherent emission too. To get incoherent radiation, there is no need to use expensive lasers - some kind of cheaper solution can be developed that could work even at room temperature. Incoherent radiation can be produced with a simple quantum well that is pumped by lateral current. The radiation is then generated in spontaneous radiative transitions between size-quantized states requiring only the electron excitation to higher subbands. No population inversion is needed.

Quantum wells have also a broad range of applications. There have been manufactured AlGaAs/GaAs based LEDs, using single and double heterostructures [2]. These heterostructures are used in high-effective red LEDs. A drawback of AlGaAs/GaAs based LEDs is the requirement of very thin GaAs quantum wells surrounded by AlGaAs barriers. An example usage of quantum wells in LEDs is showed in fig. 1.1.

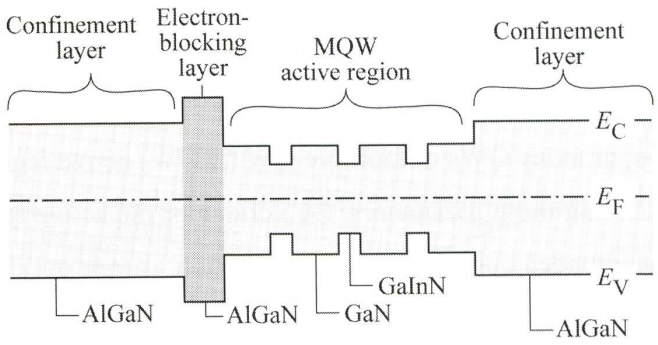

Figure 1.1: An example application of quantum wells in Light Emitting Diodes. The multiple quantum wells act there as active region and increase the efficiency of light generation. Source: fig. 4.14 (a) in [2]

Emission generated by rectangular quantum well will have relatively wide spectrum, being quite inefficient. To improve the bandwith and make it comparatively narrow, a parabolic well should be used. Parabolic quantum wells have equal energy spacings and in such wells the only strong optical transitions are between adjacent states. Bandwith of such emitters is limited by the spontaneous emission width.

In reality it is very difficult to produce parabolic quantum wells, as the doping concentration needs to be changed homogeneously. One solution of producing parabolic wells could be by digital

grading. It means the shape of parabolic well is replaced by rectangular layers of two materials giving the behaviour of real parabolic quantum well (i.e. equidistant energy levels). Preparing such a digitised parabolic well is presented here in the second part of chapter 2.

To make such parabolic well emitting spontaneous radiation, external bias should be applied to it. External bias will produce lateral electric field that gives additional kinetic energy to electrons. Additional kinetic energy increases the probability that electron jumps to higher energy levels via scattering process. This is therefore the excitation process via lateral electric field and it is described in the second part of the thesis, in chapter 3.

Chapter 2

Time-independent Schrödinger equation numerical solution methods. Application to digitally graded GaAs/AlGaAs parabolic quantum wells

2.1 Introduction

This chapter is based on paber [BEC] and describes developing of methods to find digitally graded GaAs/AlGaAs parabolic quantum well and corresponding energy eigenvalues and wave functions.

To find the band structure, the basic time-independent 1D Schrödinger equation (see eq. 2.101 in [3]) is used:

$$-\frac{\hbar^2}{2m^*(z)}\frac{\partial^2}{\partial z^2}\psi(z) + V(z)\psi(z) = E\psi(z)\,, \tag{2.1}$$

where $m^*(z)$ is the effective mass that depends on the coordinate (whether it is GaAs or AlGaAs at that point), $\psi(z)$ is the wave function, and E the energy eigenvalue. For thin potential barriers a more precise form of this equation with differential mass is preferable (see eq. 2.96 in [3]):

$$-\frac{\hbar^2}{2}\frac{\partial}{\partial z}\frac{1}{m^*(z)}\frac{\partial}{\partial z}\psi(z) + V(z)\psi(z) = E\psi(z)\,. \tag{2.2}$$

The solutions of Schrödinger equation are the energy eigenvalues and corresponding wave functions that let us to do the electron transport calculations. Knowing of energy eigenvalues help us to find the sufficient design suitable for digitally graded parabolic well that could give the best approach to ideal parabolic well. It is known that parabolic wells give equally spaced energy levels, therefore similar equal spacing is needed to be found by constructing suitable digital grading. The solutions are also needed to do the carrier transport calculations, which are described in the next chapter.

Two different methods to solve Schrödinger equation was experienced to find better accuracy. First method tried was shooting method and the other one matrix eigenvalue and eigenstates solving method, both described in Paul Harrison's book Quantum Wires, Wells, and Dots[3].

2.2 Choosing suitable numerical method

2.2.1 Shooting method

Shooting method is based on solving differential representation of Schrödinger equation having initial values that are known (see eq. 1.107 [4]):

$$\psi\left(z+\delta z\right) = \left[\frac{2m^*(z)}{\hbar^2}\left(\delta z\right)^2\left(V\left(z\right)-E\right)+2\right]\psi\left(z\right) - \psi\left(z-\delta z\right) \quad . \tag{2.3}$$

In this differential equation it is clearly visible that three consecutive points in the wave function ψ depend on each other. Energy E is the parameter that is searchable and it's value is being searched by boundary condition $\psi(z \to \infty) \to 0$. As differential equation unites three points, two of them needs to be given as the initial values. When these initial values are known, the final value for $\psi(z_n)$ can be calculated by repeating the funcion iteratively $9n - 2$ times.

Two initial values depend on the symmetry of the concrete wave function. The potential shape needs to be symmetrical to solve the Schrödinger equation using shooting method. Solving of the differential equation needs to be started from the centre of potential. If the potential is symmetrical, the wave functions can either be symmetrical or antisymmetrical (see fig. 2.1).

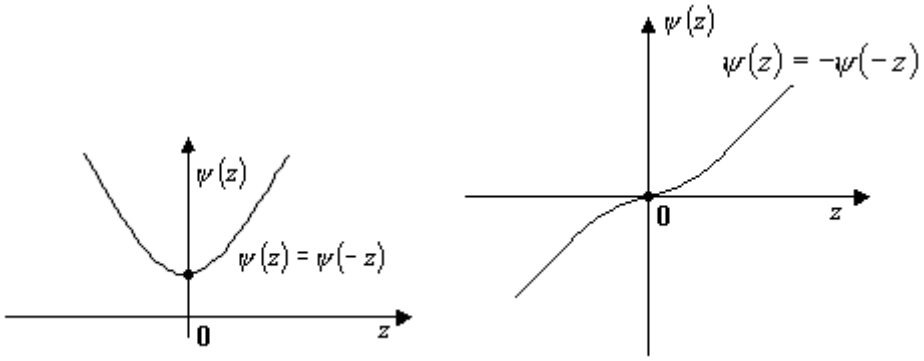

Figure 2.1: Comparison of symmetric (left) and antisymmetric (right) wave functions.

The inital values need therefore to be chosen according to the type of symmetry of wave function. For symmetrical and antisymmetrical wave function the initial values are (respectively):

$$\begin{cases} \psi(0) = 1 \\ \psi(\partial z) = 1 \end{cases}, \text{ and} \tag{2.4}$$

$$\begin{cases} \psi(0) = 0 \\ \psi(\partial z) = 1 \end{cases}. \tag{2.5}$$

As shooting method uses differential equation, the wave function is very precise near the initial values at $z = 0$ and $z = \partial z$. The final part of wave function tends to deflect from the boundary condition $\psi(z \to \infty) \to 0$ as finding the precise E that matches to the real eigenvalue is very complicated. The real values have always a definite precision, which makes it impossible to find the precise value for energy. The fact that the final part of wave function depend on the values in the beginning part of wave function makes also sense. Therefore it is very complicated to find solutions that are precise enough using shooting method, as conformance to outer boundary conditions is not very easily achievable.

Trials to solve the task using shooting method considered therefore to be too inaccurate. The values of wave functions were checked using orthogonality condition ($\int_{i \neq j} \psi_i \psi_f dz = 0$) and found that $\int_{i \neq j} \psi_i \psi_f dz \approx 0.1$ while $\int \psi_i \psi_i dz = 1$. That means the orthogonality was quite poor and this method needed to be replaced.

2.2.2 Energy and wave function coupled solution Newton method

One way to improve the results of shooting method was applying an another method to them. In [ESTSCIPROC] a method called *energy and wave function coupled solution method (EWC)* was introduced which is very precise but needs initial energies and wave functions as input. Those input values can therefore be prepared with shooting method.

EWC method solves Schrödinger equations system with clearly fixed boundary conditions - both ends of wave function can be fixed to some initial value. Both, energy eigenvalues and wave functions are calculated simultaneously. The method bases on 3-point scheme of spatial discretisation that corresponds to equation derived from Schrödinger equation (2.1):

$$-\frac{\hbar^2}{2m}\left(\frac{\psi_{i+1} - \psi_i}{\Delta x} - \frac{\psi_i - \psi_{i-1}}{\Delta x}\right)\frac{1}{\Delta x} + V_i\psi_i = E\psi_i\,, \tag{2.6}$$

where ψ_i denotes $\psi(x_i)$ and $V_i \equiv V(x_i)$. The exact boundary conditions for outer calculation area of ψ is fixed to zero (i.e. $\psi_1 = \psi_N = 0$). This boundary condition corresponds to assumption of infinitive external barriers as they cause wave function to go to zero on the borders.

This is the representation with constant or slowly changing mass. In case of dynamic mass it goes inside the brackets, as it can be seen in the following form:

$$-\frac{\hbar^2}{2}\left(\frac{\psi_{i+1}-\psi_i}{m_{i+\frac{1}{2}}\Delta x}-\frac{\psi_i-\psi_{i-1}}{m_{i-\frac{1}{2}}\Delta x}\right)\frac{1}{\Delta x}+V_i\psi_i=E\psi_i\,, \tag{2.7}$$

where $m_{i+\frac{1}{2}}$ (and $m_{i-\frac{1}{2}}$) is the average mass between m_i and m_{i+1} (m_i and m_{i-1} respectively).

EWC method calculates not the energies and wave functions directly but only their corrections. That makes it more optimal as it is not necessary to carry the absolute values through the calculations. The cycle of calculations is iterative, and can be stopped when the results do not change much anymore.

The equation 2.7 can be converted to a representation that allows it to be calculated using following equations:

$$Y=\tilde{Y}+\delta Y\,, \tag{2.8}$$

$$[\partial F/\partial Y]\times\delta Y=-\tilde{F}\,, \tag{2.9}$$

where $\tilde{Y}$ denotes the approximate unknown vector, δY is the correction vector, $\tilde{F}\equiv(\tilde{F_1},\tilde{F_2},...,\tilde{F_N})^T$ is the RHS vector of the system calculated by $\tilde{Y}$ and $[\partial F/\partial Y]$ is the $N\times N$ Jacobi matrix with the Newton method derivatives ([ESTSCIPROC]). The Jacobi matrix $[\partial F/\partial Y]$ has a triagonal structure where first row and column are additionally filled out too. The first element of main diagonal is zero. For example, for the constant mass formulation shown in eq. 2.6 the matrix has the following structure:

$$[\partial F/\partial Y]=\begin{bmatrix}
0 & 2\psi_2 & 2\psi_3 & 2\psi_4 & \cdots & 2\psi_{N-3} & 2\psi_{N-2} & 2\psi_{N-1} & 2\psi_N \\
\psi_2 & a_2 & c & 0 & \cdots & 0 & 0 & 0 & 0 \\
\psi_3 & c & a_3 & c & \cdots & 0 & 0 & 0 & 0 \\
\psi_4 & 0 & c & a_4 & \cdots & 0 & 0 & 0 & 0 \\
\vdots & \vdots & \vdots & \vdots & \ddots & \vdots & \vdots & \vdots & \vdots \\
\psi_{N-3} & 0 & 0 & 0 & \cdots & a_{N-3} & c & 0 & 0 \\
\psi_{N-2} & 0 & 0 & 0 & \cdots & c & a_{N-2} & c & 0 \\
\psi_{N-1} & 0 & 0 & 0 & \cdots & 0 & c & a_{N-1} & c \\
\psi_N & 0 & 0 & 0 & \cdots & 0 & 0 & 0 & 1
\end{bmatrix}, \tag{2.10}$$

where $c\equiv\hbar/(2m\Delta x^2)$ and $a_i\equiv E-V_i-2c$. To get deeper overview of this method, see [ESTSCIPROC].

This method is very precise, as by the end of iterations the increment vector δY approaches to computer zero. The disadvantages of this method are first, the need to obtain the initial guess for wavefunction, and second, the possibility to skip some eigenvalues. Thereby for rather difficult multibarrier digitised quantum well the method was decided not to be used. Using more common methods for trivial eigenvalue problems could solve these disadvantages, which is the topic of next subsection.

2.2.3 Method based on matrix eigenvalue standard solvers

This method is based on classical linear algebra methods that are meant for finding eigenvalues and eigenvectors of matrices. This will be much more precise than shooting method, because the elements do not depend on each other any more. To solve the Schrödinger equation (2.1) using matrices, the equation needs to be modified to differential representation. The following representation is taken from [3, eq. 3.53, page 89]:

$$\frac{1}{m*(z+\delta z/2)}\psi(z+\delta z)=\left(\frac{2(\delta z)^2}{\hbar^2}[V(z)-E]+\frac{1}{m*(z+\delta z/2)}+\frac{1}{m*(z-\delta z/2)}\right)\psi(z)-$$

$$-\frac{1}{m*(z-\delta z/2)}\psi(z-\delta z)\,. \tag{2.11}$$

The equation 2.11 is differencial, which means, it connects three consecutive wave function values. To solve it, standard eigenvalue and eigenvector computing methods can be used and the equation needs to get matrix representation. The first step should be rewriting the equation to the following form:

$$-\frac{1}{m^*\left(z_{i-\frac{1}{2}}\right)}\psi_{i-1}+\left\{\frac{2\left(\delta z\right)^2}{\hbar^2}V\left(z_i\right)+\frac{1}{m^*\left(z_{i+\frac{1}{2}}\right)}+\frac{1}{m^*\left(z_{i-\frac{1}{2}}\right)}\right\}\psi_i-\frac{1}{m^*\left(z_{i-\frac{1}{2}}\right)}\psi_{i+1}=\frac{2\left(\delta z\right)^2}{\hbar^2}E\cdot\psi_i\,, \tag{2.12}$$

where $\psi_i=\psi\left(z\right)$, $\psi_{i\mp1}=\psi\left(z\mp\delta z\right)$, $z_i=z$ and $z_{i\mp\frac{1}{2}}=z\mp\delta z/2$. For eigenvalue problem it is better to present this equation without the coeficient in front of energy E. Therefore the whole equation needs to be multiplied by $\frac{\hbar^2}{2(\delta z)^2}$ and will get the following form:

$$-\frac{k}{m^*\left(z_{i-\frac{1}{2}}\right)}\psi_{i-1}+\left\{V\left(z_i\right)+\frac{k}{m^*\left(z_{i+\frac{1}{2}}\right)}+\frac{k}{m^*\left(z_{i-\frac{1}{2}}\right)}\right\}\psi_i-\frac{k}{m^*\left(z_{i-\frac{1}{2}}\right)}\psi_{i+1}=E\cdot\psi_i\,, \tag{2.13}$$

where k denotes the coeficient $\frac{\hbar^2}{2(\delta z)^2}$.

The coeficients before ψ-s can be placed into a symmetric tridiagonal band matrix and the task can be reformulated as a standard eigenvalue problem:

$$[A]\cdot[\psi]=E[\psi]\,, \tag{2.14}$$

where $[A]$ is the $N\times N$ matrix, $[\psi]$ is a column vector with N elements, and E is the wanted energy eigenvalue. By solving this eigenvalue problem with standard software (e.g. *dstev* and *dstevx* in LAPACK[1]), the energies E_l (eigenvalues) and corresponding wave functions ψ_l (eigenvectors) can be found (where l is the number of energy level, $l=1...N_l$).

The orthogonality of the wave functions is much better using this method. The value of nondiagonal elements of orthogonality matrix was $\int_{i\neq j}\psi_i\psi_f dz\approx10^{-9}$, which shows clearly how much this method is better than shooting method.

2.2.4 Comparison of all three methods

The comparison of the main properties, and pros and cons of all these methods are listed in tables 2.1 and 2.2.

Table 2.1: Comparison table of all three methods. N is the number of net points

Property	**Shooting method**	**Newton method**	**Matrix eigenvalue method**
1. Boundary conditons	One side is fixed with 2 pts	Both sides fixed to 0	Neither sides fixed
2. Wave function orthogonality	$\approx10^{-1}$	$\approx10^{-12}$	$\approx10^{-9}$
3. Time efficiency	Medium (time $\sim N$)	Very High (time $\sim N$)	High (time $\sim N^3$)
4. Initial guess for wave function	Not needed	Needed	Not needed
5. Implementation complexity	Medium	High	Low
6. Traceability	Good	Poor	Poor
7. Other assumptions	Symmetrical potential needed	Outer barriers are infinitively high	Not very clear boundary conditions

[1]LAPACK is an acronym of words *Linear Algebra PACKage*. See http://www.netlib.org/lapack for more information.

Table 2.2: Advantages and disadvantages of the three methods

Method	Advantages	Disadvantages
Shooting method	Easy to implement	Not very precise; May skip energy levels if they are too close to each other
Newton method	Boundaries fixed to 0; Relatively fast	Initial guess for energies and wave functions needed; May skip energy levels if they are too close to each other
Matrix eigenvalue method	Standard implementation	Not very clear boundary conditions

2.3 Optimising digitally graded potentials

2.3.1 Introduction

The main task in this chapter is to find digitally graded potential layout that could be a good approximation to parabolic quantum well. On the cover an example parabolic well with digital grading is shown. Digital grading is needed to simplify the production process of parabolic quantum well devices. It is technologically very complicated to manufacture quantum wells that have parabolic shape. One possibility to overcome this obstacle is digitalisation of the parabolic well. This means the two materials used in parabolic well (GaAs and $Al_xGa_{1-x}As$) are altered as many times as necessary to achieve similar behaviour as true parabolic well has. Finding the right digital grading can be time consuming, because all the thick layers must be carefully shifted left and right to find the best approach to equal spacing between energy levels. The spacing is as a feedback in digitised parabolic well construction method.

2.3.2 Building initial potential

Building the initial structure was relatively easy. The first criteria while building the structure, was the integral of the potential function (the area) that needs to be equal for both cases - for original parabolic well and for digitised well. This defined the number of layers. The second criteria was needed to define their initial placement. The algorithm of assigning the layers to their initial places started moving from the centre of potential and integrated over the original potential well. If the integral occured to exceed the area of one monolayer, a layer was put into this place where it happened. Then, the counter was zeroed and integration continued until the end of the potential. Initial potential was behaving more or less like parabolic well but it was still not very precise.

2.3.3 Optimising the potential

To optimise the initial potential, there were several algorithms tried. The first and easiest was to move layers one step[2] left and right, doing it one by one with each of the layers. After each movement the unified spacing parameter between energy levels was calculated again and compared to current minimal spacing parameter. This process was continued with several other algorithms too until the spacing didn't improve any more.

To characterise the deviation of spacings from wanted value, a statistical parameter - *Root Mean Square* (*RMS*) - was used. The parameter was calculated using the following equation:

$$RMS = \sqrt{\frac{\sum_{i=1}^{N-1} \left(\Delta E_{i,i+1} - \Delta E_{\text{wanted}}\right)^2}{N-1}}, \tag{2.15}$$

where $\Delta E_{i,i+1} = E_{i+1} - E_i$ is the spacing between energy levels i and $i+1$, ΔE_{wanted} is the wanted energy spacing (constant value), and N is the number of energy levels. After each movement of

[2] the width of a monolayer (0.2825 nm)

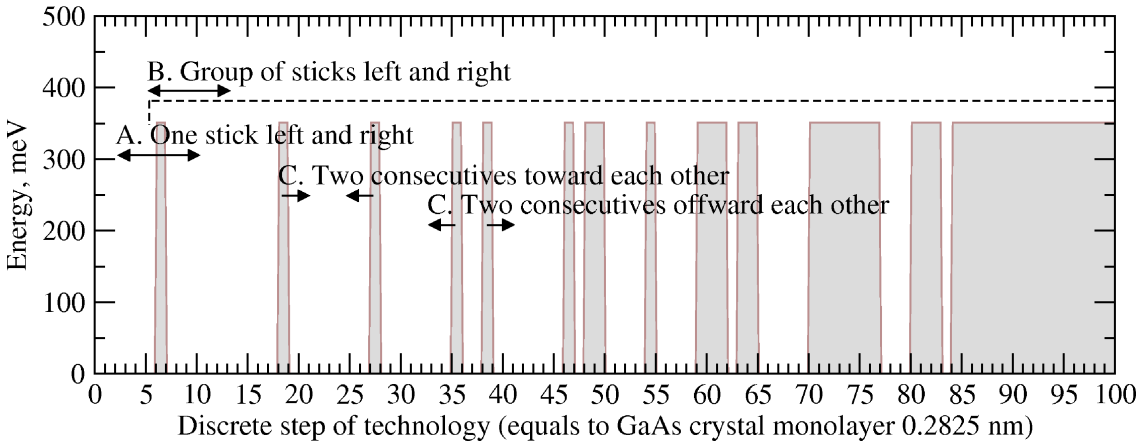

Figure 2.2: The algorithms used to find adequate quasi-parabolic quantum well using digital grading of two substrates. The shifts are done symmetrically for both sides.

a layer the RMS is recalculated and used in later movements as comparison. If a new movement improved the RMS, the movement fixated and another layer took into the focus.

The list of all algorithms used is described below and shown in fig. 2.2.

A. Moving one stick at a time to the left and right. This was the first method tried to improve the RMS of energy level spacings. The algorithm started from the centre of potential and moved symmetrically to the direction of the edge. When it reached the end, it started coming back reversely to the centre. The algorithm continued this cycle until the movings of layers do not improve the energy spacings any more.

If the new position of a layer is occupied by another layer, then this layer will also be moved on. If there are many layers, then all of them will be moved.

B. Moving a group of sticks to the left and right. This method was the first improvement to the previous one as it did not give the best approach. The method starts again from the middle of the well and goes to the side. First moving incorporates all the layers that are moved to the right and to the left. The second moving leaves out the first layer and takes all the others ($n-1$ if n is the number of layers) with.

C. Moving two consecutive sticks towards and away from each other. This was the latest improvement tried to do the achieved results even better. The process starts again from the middle of the well and goes to the side. All the consecutive layers were moved towards each other and then away from each other.

In final calculations all the methods were combined, alternating them after each step. Acting that way gave the best result - the precision of energy spacings came around 5 percent what was the first goal.

2.4 Conclusion

There are two main results achieved in this chapter. The aim of the first task was to find a proper method for band structure calculation. This task was done successfully - a standard linear algebra method to find matrix eigenvalues and eigenvectors was chosen to be the best one. The initial data was chosen such, that the eigenvalues were the energy values and eigenvectors the corresponding wave function.

The second task in this chapter was to find a good approximation to parabolic quantum well using digital grading i.e. alteration of two different substances GaAs and AlGaAs. After the layout of layers was fixed - the energy levels had more or less equal spacing, the final results was to be calculated. After the final energy eigenvalues and wave functions were ready, the process continued with carrier transport calculations, which is handled in the next chapter 3.

Three scientific papers have been published on this topic, they are presented in the appendixes.

Chapter 3

Lateral transport task of quantum well based broadband terahertz emitter

3.1 Introduction

This chapter is based on manuscript submitted to Journal of Applied Physics [JAP] and describes developing of methods to calculate emission rates for lateral transport of charge carriers.

The quantum wells we are using are two dimensional, which means that the electrons have two directions where it can move and one direction where it is fixed. This is therefore called in-plane electron transport. In fig. 3.1 it is showed how the electrons can move along the valley (y-axis) and up along the subband (x-axis). Along the y-axis the electrons are fixed and can not move.

Lateral transport brings up the effect of scattering, which means the electrons are colliding with lattice atoms. Electric field caused by such collisions heats the electrons up giving them higher kinetic energy. That will cause the electrons to climb up along the subband until they will collide with lattice and go to higher subband by scattering process (see fig. 3.2). Higher subbands will therefore get higher population of electrons. Electrons in excited subbands will then relax into lower ones and produce spontaneous emission of photons. The main idea is therefore in increasing the output power by additional spontaneous emission.

Using this idea, a device emitting terahertz radiation can be built. An example of such device can be seen in fig. 3.3.

The lateral electric field causes therefore the Fermi-Dirac distribution function needed in transport calculations to shift along the energy axis to some extent (see fig. 3.4 and section 3.2). The original distribution function for equilibrium is given by (see eq. 2.49 in [3]):

$$f^{\mathrm{FD}}(E) = \frac{1}{\exp\left[\left(E - E_F\right)/kT\right] + 1}, \tag{3.1}$$

where E_F is the Fermi energy.

3.2 Shifted Fermi-Dirac distribution function

The internal electric field of lateral transport causes electrons to get a remarkable drift velocity ($v_d > 0$) heating themselves up. This will cause the Fermi-Dirac distribution function to shift along the E axis by energy that corresponds to v_d (see eq. 3.1). The distribution function will get the following form then:

$$f^{\mathrm{sFD}}(\mathbf{k}) = \left[1 + \exp\frac{E_{n0} + \frac{\hbar^2\left(\left(k_x - k_0(F,T_{\mathrm{latt}})\right)^2 + k_y^2\right)}{2m^*} - E_{F_n}}{k_B T_{\mathrm{el}}(F,T_{\mathrm{latt}})}\right]^{-1}, \tag{3.2}$$

where $\mathbf{k} = (k_x, k_y)$ is the in-plane wave vector that is proportional to energy E in the original equation, E_{n0} is the subband minimum energy, E_{F_n} is the quasi-Fermi level of n-th subband, k_0

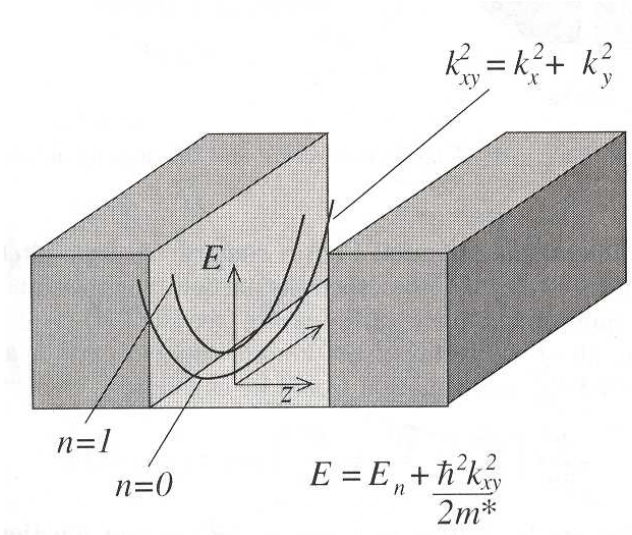

Figure 3.1: In-plane dispersion curves and the subband structure. Source: fig. 2.5 in [3].

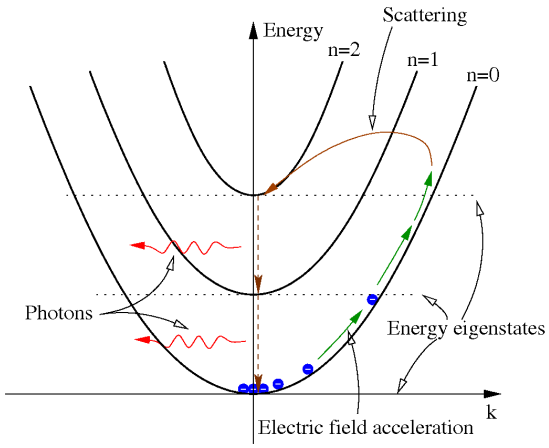

Figure 3.2: Model of subband excitation and relaxation processes. Nonradiative intersubband scattering processes (polar LO phonons and acoustic deformation potential phonons) cause electron transitions between subbands. Lateral electric field accelerates electrons within every subband. Optical radiation output is caused by spontaneous drop of electrons from higher subbands to lower ones.

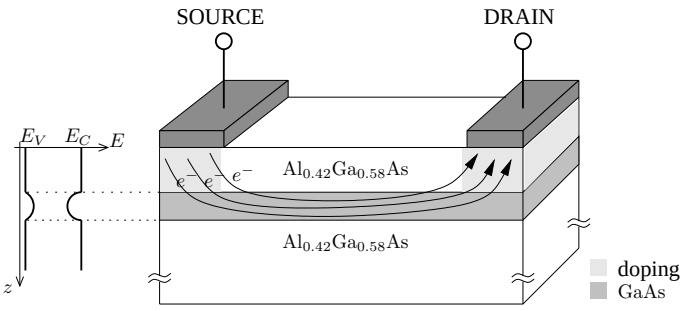

Figure 3.3: An example device based on a laterally pumped quantum well

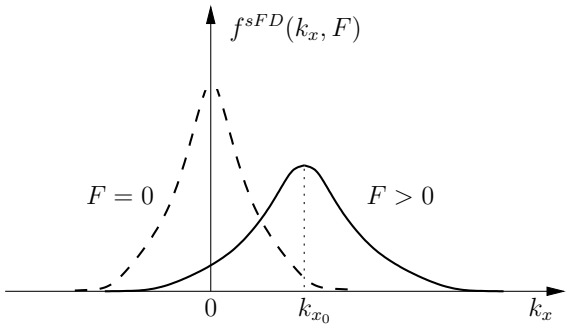

Figure 3.4: The shifted Fermi-Dirac distribution function with effective electron temperature. The shift is caused by lateral electric field, and the flatness is caused by the increase of temperature.

is the drift wave vector (along the x-axis), and T_{el} the heated electron temperature. k_0 and T_{el} depend both on the electric field F and lattice temperature T_{latt}.

Two unknown parameters are introduced with *shifted* distribution function, drift wave vector and electron temperature (k_0 and T_{el}), both functions of applied electric field F and lattice temperature T_{latt}. These functions decided to be taken from literature, as there are several researches done on this matter already.

Dependence between drift velocity and electric field is taken from [5]. The relevant figure is 3.5 (left one) which is a copy of original figure from the paper. The points on this graph were carefully written out and interpolated using Lagrange's interpolation method. The interpolated data were then written out again and is presented here as the right curve in the same figure. It can be seen, that the result comforms more or less to the original data. Experiments showed that this small difference does not affect the overall result significantly. In calculations, where the wave vector k is used instead of speed v, the conversion can be done using equation:

$$k\left(F\right) = \frac{m^* \cdot v\left(F\right)}{\hbar}. \tag{3.3}$$

The electron temperature and electric field dependence is also taken from the same paper. Fig. 4 in [5] shows the dependency between electric field and average energy for GaAs at 300 K. The comparison is presented in fig. 3.6 where both, the original and interpolated curves are presented. The average energy E is converted to temperature T using following equation:

$$T\left(F\right) = \frac{2E\left(F\right)}{3k_{\mathrm{B}}}. \tag{3.4}$$

3.3 Calculation methodology

3.3.1 Overview

The process of calculations is described in the figure 3.7. The calculation has two cycles - inner one is iterative to find the proper subband populations, and outer one that is over the electric field values. The band structure needs to be calculated manually in advance.

3.3.2 Calculation of raw scattering rates

If an electron is moving within a crystal lattice, it will sooner or later collide with the lattice atoms. Electrons can change their states that way - collisions may either increase or decrease their energy. According to the *Fermi's Golden Rule* the scattering process is described as following: if an electron in a state $|i\rangle$ with energy E_i experiences a time-dependent perturbation $\tilde{\mathcal{H}}$ which could transfer it to a state $|f\rangle$ with energy E_f, the lifetime of the carrier in state $|i\rangle$ is (according to eq 8.1 in [3]):

$$\frac{1}{\tau_i} = \frac{2\pi}{\hbar} \sum_f \left| \langle f | \tilde{\mathcal{H}} | i \rangle \right|^2 \delta\left(E_f - E_i\right). \tag{3.5}$$

There are several types of scatterings, but only longitudinal optic and acoustic deformation potential are used, as the others do not affect very much the results. All the scattering types

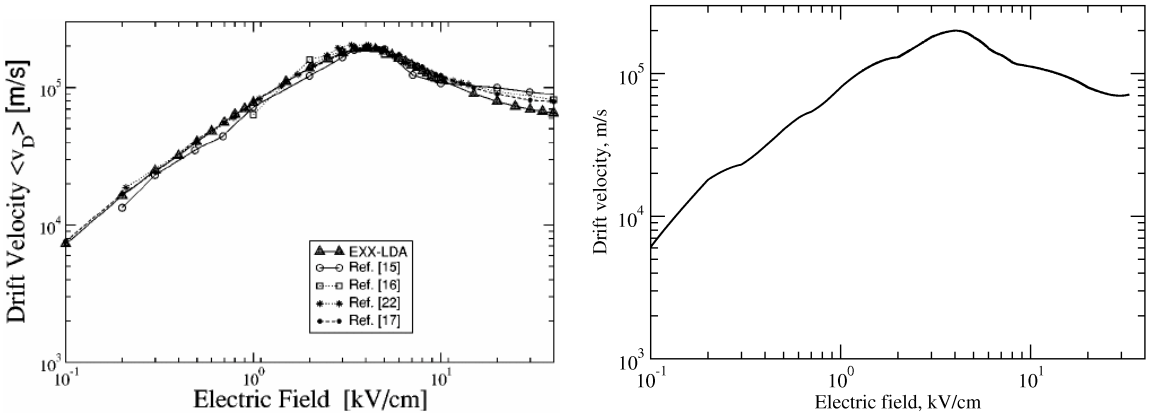

Figure 3.5: Comparison of the original (left) and interpolated (right) dependency between drift velocity and electric field at 300 K in GaAs (source: fig. 3 in [5]).

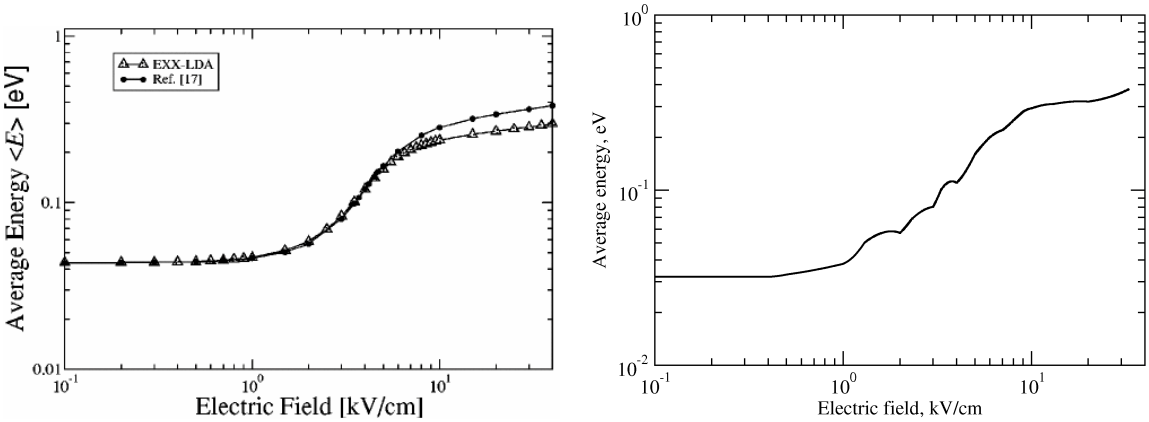

Figure 3.6: Comparison of the original and the interpolated dependency between average energy and electric field at 300 K in GaAs (source: fig. 4 in [5]).

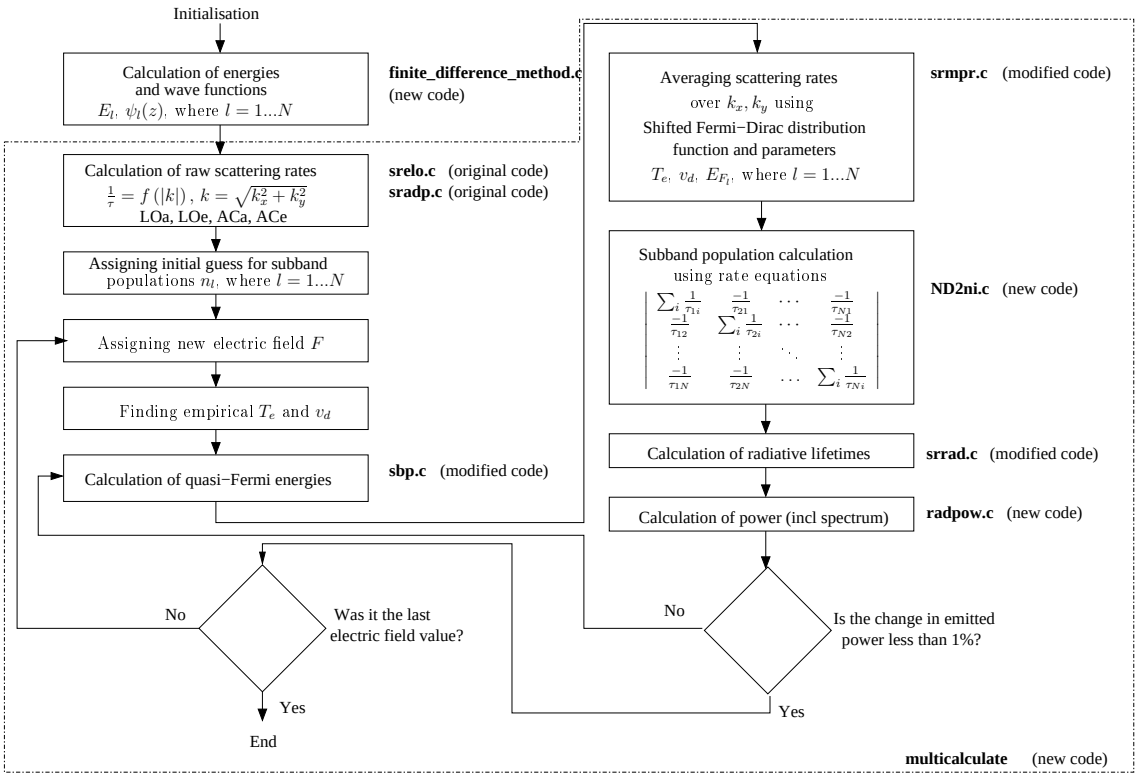

Figure 3.7: Overview of the calculation process. The source of codes given mean: *original* - code taken from [3], *modified* - code taken from [3] and modified by the author, and *new* - code written by the author. Variable N means the total number of energy levels (subbands). The majority of the calculations are automated using a program called **multicalculate**.

have their own equations for the perturbation $\tilde{\mathcal{H}}$, which gives the final form to the scattering rate equations described below.

The calculation of longitudinal optic phonon scatterings are done using Paul Harrison's book (section 8.4 in [3]). According to this section, the scattering rate equation 3.5 can be improved and will finally get the following form (see eq. 8.147 in [3]):

$$\frac{1}{\tau_i} = \frac{m^* e^2 \omega P'}{(2\pi)^2 \hbar^2} \int_{-\infty}^{\infty} \frac{\pi \left|G_{\text{if}}(K_z)\right|^2}{\sqrt{K_z^2 + 2K_z^2\left(2k_i^2 - \frac{2m^*\Delta}{\hbar^2}\right) + \left(\frac{2m^*\Delta}{\hbar^2}\right)^2}} \mathrm{d}K_z\,, \tag{3.6}$$

where Δ is the sum of subband minimal energy and the kinetic energy within the band $E_f - E_i \mp \hbar\omega$ (the upper sign in front of $\hbar\omega$ represents the emission of a phonon and lower the absorption), $P = \left(\frac{1}{\epsilon_\infty} - \frac{1}{\epsilon_s}\right)\left(N_0 + \frac{1}{2} \mp \frac{1}{2}\right)$ (where ϵ_∞ and ϵ_s are the high- and low-frequency permittivities of the material, and $N_0 + \frac{1}{2} \mp \frac{1}{2}$ represents the number of phonons per unit area within the crystal, having minus in case of absorption and plus in case of emission, where N_0 is the Bose-Einstein factor), K_z and ω are the wave vector (along the growth axis) and angular frequency of the phonons, k_i is the momentum of phonon in the initial state, and $G_{\text{if}} = \int \psi_f^*(z)\, \mathrm{e}^{-iK_z z} \psi_f^*(z)\, \mathrm{d}z$ is the *form factor* of scattering events.

Scattering rate acoustic deformation potential calculations (AC) were done using section 9.9 in Paul Harrison's book [6]. The equation for AC scattering is in the form (see eq. 9.186 in [6]):

$$\frac{1}{\tau_i}(k_i) = \frac{D_A^2 m^*}{\rho v_s (2\pi)^2 \hbar^2}\left(N_0 + \frac{1}{2} \mp \frac{1}{2}\right) \int_0^{\infty}\int_0^{2\pi} \left(G_{\text{if}}(K_z)\right)^2 \times$$
$$\times \left(\frac{\Theta(\alpha_1)\,\alpha_1\sqrt{\alpha_1^2 + K_z^2} + \Theta(\alpha_2)\,\alpha_2\sqrt{\alpha_2^2 + K_z^2}}{\alpha_1 - \alpha_2}\right) \mathrm{d}\phi \mathrm{d}K_z\,, \tag{3.7}$$

where D_A is *electron acoustic deformation potential* (in case of Γ-valley of GaAs $D_A = 7.0\,\text{eV}$. Source: Table 2.1 in [7]), G_{if} is the form factor of scattering events (see previous paragraph),

$\alpha_{1,2} = -k_i \cos\phi \pm \sqrt{k_i^2 \cos^2\phi - \frac{2m^*\Delta E}{\hbar^2}}$ (according to eq. 9.182 in [6]), k_i is the phonon wave number of inital subband, K_z is the wave vector of the phonons, Θ is the Heaviside function, ρ and v_s are the density and speed of sound (respectively) in GaAs, and $N_0 + \frac{1}{2} \mp \frac{1}{2}$ represents the number of phonons per unit area within the crystal, having minus in case of absorption and plus in case of emission (where N_0 is the Bose-Einstein factor).

There is a standard implementation to solve these tasks, presented in the books. A program called **srelo.c** is meant for LO scattering calculations and **sradp.c** for AC scattering. Therefore in the overall calculation process, this part was solved using these standard programs.

3.3.3 Calculation of quasi-Fermi energies

In calculation of mean scattering rate (subsection 3.3.4), the shifted Fermi-Dirac distribution function is constructed. According to the equation 3.1, the Fermi-Dirac distribution function depends on Fermi energy E_F. In lateral transport the Fermi energy is sepparate for all the subbands:

$$f_i^{\mathrm{FD}}(E) = \frac{1}{\exp\left[\left(E - E_{F_i}\right)/kT\right] + 1}\,, \tag{3.8}$$

where the index i expresses the number of subband. Fermi energy is therefore a 'quasi' energy describing the carrier population within a subband.

Quasi-Fermi energies need to be calculated for the *shifted* distribution function in next subsection. As the Fermi energy is tightly related to carrier population within one subband, the problem can be solved using the equation 2.48 in [3]. The equation will give the electron occupation of a state i:

$$n_i = \frac{m^*}{\pi\hbar^2} \int_{\mathrm{subband}} f_i^{\mathrm{FD}}(E)\,\mathrm{d}E\,. \tag{3.9}$$

By putting equations 3.8 and 3.9 together, the Fermi energies can be found using reverse search method if the subband populations are known. The subband populations will be calculated later in subsection 3.3.5. This is not problem that they are calculated in reverse order, because of the iterative calculation. In the first round, arbitrary populations are used.

In Paul Harrison's book [3], the method was implemented for equilibrium (a program called **sbp.c**). The script was modified to provide *shifted* Fermi-Dirac distribution function for the non-equilibrium.

3.3.4 Calculation of mean scattering rates

Calculation of subband populations in next subsection (3.3.5) depends on mean scattering rates. Therefore it is necessary to find the mean rates using equation 8.149[1] from Paul Harrison's book [3]:

$$\left\langle \frac{1}{\tau_{if}} \right\rangle = \frac{\int \frac{1}{\tau_{if}} f_i^{\mathrm{FD}}(E)\left(1 - f_f^{\mathrm{FD}}\left(E \mp E_{\mathrm{phonon}}\right)\right)\mathrm{d}E}{\int f_i^{\mathrm{FD}}(E)\,\mathrm{d}E}\,, \tag{3.10}$$

where the indexes i and f stand for 'initial' and 'final' states, and E_{phonon} is the phonon energy having minus in case of emission and plus in case of absorption.

As lateral transport shifts the distribution function away from the zero, it's shifted form should be used in this equation too. The integral over energy have also to be changed to integral over wave vector $\mathbf{k}$ then. In computational implementation, the equation will look like this:

$$\left\langle \frac{1}{\tau_{if}} \right\rangle = \frac{\int_{k_x}\int_{k_y} \frac{1}{\tau_{if}} f_i^{s\mathrm{FD}}(k_x,k_y)\left(1 - f_f^{\mathrm{FD}}\left(E - \mp E_{\mathrm{phonon}}\right)\right)\mathrm{d}k_x\mathrm{d}k_y}{\int_{k_x}\int_{k_y} f_i^{s\mathrm{FD}}(k_x,k_y)\,\mathrm{d}k_x\mathrm{d}k_y}\,, \tag{3.11}$$

where $E = E_i + \frac{\hbar^2}{2m^*}\left(k_x^2 + k_y^2\right)$ (where E_i is the subband minimum energy and $\frac{\hbar^2}{2m^*}\left(k_x^2 + k_y^2\right)$ the kinetic energy), and $f_i^{s\mathrm{FD}}(\mathbf{k})$ is the *shifted* Fermi-Dirac distribution function (see section 3.2).

This function was implemented using a standard program **srmpr.c** from Paul Harrison's book [3] which was improved with the shifted distribution function.

[1] The corrected form is presented here according to the errata of the book

3.3.5 Calculation of subband populations using rate equations

To calculate the subband populations, rate equations need to be constructed using average scattering rates. It is known that the number of electrons leaving from a state is equal to the number of electrons coming to the state. Therefore the following rate equation can be used:

$$\frac{\mathrm{d}n_f}{\mathrm{d}t} = \sum_{i=1}^{N} \frac{1}{\tau_{if}} n_i - n_f \sum_{i=1}^{N} \frac{1}{\tau_{fi}} = 0\,, \tag{3.12}$$

where τ_{if}^{-1} is the total averaged scattering rate from i-th to f-th subband, n_i is the electron population of i-th subband, and N the number of subbands. This equation contains N unknown variables n_i-s, which means at least $N-1$ equations need to be found in addition to solve it. As the equation is meant for one subband only (f-th), it can be applied for all the N subbands:

$$\begin{cases} \sum_{i=1}^{N} \frac{1}{\tau_{i1}} n_i - n_1 \sum_{i=1}^{N} \frac{1}{\tau_{1i}} &= 0 \\ \sum_{i=1}^{N} \frac{1}{\tau_{i2}} n_i - n_2 \sum_{i=1}^{N} \frac{1}{\tau_{2i}} &= 0 \\ \vdots & \vdots \\ \sum_{i=1}^{N} \frac{1}{\tau_{iN}} n_i - n_N \sum_{i=1}^{N} \frac{1}{\tau_{Ni}} &= 0 \end{cases}. \tag{3.13}$$

Unfortunately, in this case, zero populations will also give a true result ($n_i = 0$, $i = 1...N$). Therefore an additional equation which connects the subband populations to overall electron concentration in the semiconductor should be introduced:

$$n_1 + n_2 + n_3 + \cdots + n_N = N_D\,, \tag{3.14}$$

where N_D is the overall density of electrons.

These equations can easily be solved using the following matrix equation

$$Ax = y\,, \tag{3.15}$$

where

$$A = \begin{vmatrix} \sum_i \frac{1}{\tau_{1i}} & \frac{1}{\tau_{21}} & \cdots & \frac{1}{\tau_{(N-1)1}} & \frac{1}{\tau_{N1}} \\ \frac{1}{\tau_{12}} & \sum_i \frac{1}{\tau_{2i}} & \cdots & \frac{1}{\tau_{(N-1)2}} & \frac{1}{\tau_{N2}} \\ \vdots & \vdots & \ddots & \vdots & \vdots \\ \frac{1}{\tau_{1(N-1)}} & \frac{1}{\tau_{2(N-1)}} & \cdots & \sum_i \frac{1}{\tau_{(N-1)i}} & \frac{1}{\tau_{N(N-1)}} \\ 1 & 1 & \cdots & 1 & 1 \end{vmatrix}, \; x = \begin{vmatrix} n_1 \\ n_2 \\ \vdots \\ n_{N-1} \\ n_N \end{vmatrix}, \text{ and } y = \begin{vmatrix} 0 \\ 0 \\ \vdots \\ 0 \\ N_D \end{vmatrix}.$$

To solve this task, a new program **ND2ni.c** was written.

3.3.6 Calculation of emission characteristics

The emission characteristics we are interested in, is the emitted power, both the total value and the spectrum. All the cycle of calculations done before, was to find the subband populations n_i for the equation of emitted power:

$$P_{\text{total}} = \sum_{i>f}^{N} \frac{n_i}{\tau_{if}^{\text{rad}}} \frac{\hbar^2}{2m^*} \left(E_i - E_f\right)\,, \tag{3.16}$$

where n_i is the population of i-th subband, τ_{if}^{rad} is the spontaneous radiative lifetimes and $\hbar\omega_{if} = E_i - E_f$ the energy between i-th and f-th subbands. The radiative lifetime is given by:

$$\frac{1}{\tau_{if}^{\text{rad}}} = \frac{e^2 \overline{n} \left(E_i - E_f\right)^3 d_{if}^2}{3\pi\epsilon_0 c^3 \hbar^4}\,, \tag{3.17}$$

where $\overline{n}$ is the refractive index, d_{if} are the optical dipole matrix elements, $d_{if} = \int \psi_i(z)\,\psi_f(z)\,z\mathrm{d}z$. Spontaneous radiative lifetimes $\frac{1}{\tau_f^{\text{rad}}}$-s do not depend on subband populations n_i, which means they can be calculated prior to other calculations. This is important in practical implementation,

because this calculation can be omitted in the main cycle to save time. The second output needed, the power spectrum, is calculated as a well-known Lorentzian pectrum:

$$P(E) = \sum_{i>f}^{N} \frac{n_i}{\tau_{if}^{\mathrm{rad}}} (E_i - E_f) \frac{\Gamma}{\pi} \frac{1}{(E - (E_i - E_f))^2 + \Gamma^2}, \tag{3.18}$$

where Γ is the line width (half width at half maximum) of the intersubband transitions, E_i and E_f the energies of initial and final subbands, and τ_{if}^{rad} the spontaneous radiative lifetimes.

3.3.7 Overall calculation automation

According to fig. 3.7, the main cycle of transport calculations are being controlled by a program **multicalculate**. This means, the band structure needs to be calculated in advance, then the transport calculations can be started. The program asks all the input data from the user (i.e. the electric field values F_i, temperature T, and total electron density N_D) and calls the subroutines automatically with the right arguments in the right order. The program checks the change in power emission after each inner iterative calculation cycle and exits as soon as one percent of precision is achieved. All the inner iterative cycles are a part of outer cycle which runs over the array of electric fields.

3.4 Conclusion

The main problem through the development process has been the validation of the results. It is not easy to check the results as there are no easy ways to do it. As there are standard implementations (that can be trusted) for unbiased case in Paul Harrison's book [3], the results for $F = 0\,\mathrm{V/cm}$ can be compared. Calculations done for 7 THz case show that the difference is under 1 %. The comparison is given in the table 3.1.

Table 3.1: Comparison between results got by standard implementation (taken from [3]) and author's implementation. Electric field is not applied ($F = 0\,\mathrm{V/cm}$), having only black body radiation.

	77 K	300 K
Implementation taken from QWWAD ([3]). Averaging is done using equation 3.10	$16.97\,\mathrm{W/m^2}$	$16.98\,\mathrm{W/m^2}$
Implementation made by the author. Averaging is done using equation 3.11	$17.02\,\mathrm{W/m^2}$	$17.07\,\mathrm{W/m^2}$
Deviation	0.3 %	0.5 %

In the first stage of calculations done in Leeds in augumn 2007, the error in results was around 30 %. By now, the methods have been improved and corrected, so the precision has also gone better.

It can be therefore stated that the calculation method of electron transport in laterally pumped semiconductor has been developed and implemented. Two scientific papers are submitted and waiting for acceptance, [JAP] to Journal of Applied Physics, and [ITQW07] to ITQW conference (2007 in Ambleside, Cumbria, U.K.).

Chapter 4

Conclusion

The main purpose taken at the beginning of the work has been successfully completed - the methods of electron transport calculation for laterally pumped emitting device were developed and the acceptable results were obtained. Also the subpurpose of finding a propriate method to solve Schrödinger equation was done well.

It has been showed that even with one layer terahertz radiation can be emitted which power is higher than black body radiation. In [JAP] the dependence between the electric field and emitted power is showed.

In the first chapter the different methods to solve Schrödinger equation were examined. In the second chapter the division of electrons between the subbands was examined together with estimation of generated optical radiation power and spectrum. This methodology bases mainly on Leeds University methods to examine the Quantum Cascade Lasers (QCL). For this specific task where quasi-parabolic quantum wells with relatively many subbands are used, and the transport dominates (exciting with current), several additional calculation modules needed to be implemented. These were also shown in fig. 3.7.

The concrete results of this work are listed in the following:

1. The numerical solution methods for Schrödinger equation were examined and compared. The best method occured to be a standard linear algebra eigenvalue solving method. A program called **finite_difference_method.c** was implemented to calculate the energy eigenvalues and corresponding wave functions. The source code of this program can be found in the web page of this work.

2. A method was implemented to optimise the digitised quasi-parabolic quantum wells seeking the equal spacings between energy eigenvalues. For 7 THz emission frequency, the *root-mean-square* deviation of energy spacings below 4 % was achieved, which is enough for the practical approximation of parabolic quantum well.

3. Several calculation modules were realised. Some of the modules were taken from [3] (QWWAD) and re-implemented, but some of them are new. The list of re-implemented calculation modules includes:

   - **sbp.c** Calculation of quasi-Fermi energies for each subband. The base of the code was taken from [3] but it was improved for $F > 0$ case.
   - **srmpr.c** Calculation of mean scattering rates. The base of the code was also taken from [3], while the Fermi-Dirac distribution function replaced to the *shifted* FD function, also to support $F > 0$ case.
   - **srrad.c** Calculation of spontaneous radiative lifetimes. The method in the original version was improved.

   The list of newly built modules is:

   - **ND2ni.c** Calculation of subband populations using rate equations.
   - **radpow.c** Calculation of generated radiation power and spectrum.

4. The calculations were made for 7 THz structures under lattice temperatures 300 K and 77 K. The time cost for such calculations is quite high. In the early phase of calculations the time spent to find one point (output characteristics for one electric field F value) reached to 24 hours. By now, the algorithms have been optimised and the time has been decreased to 45 minutes. Therefore to make a serie of calculations (for example with 11 electric field values - 0, 1 kV/cm,...,10 kV/cm), it may take around 9 hours.

5. The 7 THz structure can produce radiation over the black body spectrum even in room temperature (300 K). In [ITQW07] it has been showed that it works even near 400 K temperature. It is known that Quantum Cascade Lasers need to work with very low lattice temperature (under 150 K), therefore this fact is very important.

Five scientific papers and manuscripts related to this work has been written. Leeds University has shown up an interest to build such broadband terahertz emitter.

The source codes written for this work have been collected and they can be found in the web page of this work - `http://home.cyber.ee/reeno/pqw`.

Bibliography

[1] K. Mizoguchi, A. Mizumoto, M. Nakayama, and et al. Characterization of terahertz electromagnetic waves from coherent longitudinal optical phonos in gaas/algaas multiple quantum wells. *Journal of Applied Physics*, 100(10), November 2006.

[2] E. Fred Schubert. *Light-Emitting Diodes*. 2003.

[3] Paul Harrison. *Quantum Wells, Wires and Dots. Theoretical and Computational Physics*. John Wiley & Sons Ltd., 2000.

[4] Paul Harrison. *Computational Methods in Physics, Chemistry and Biology*. The University of Leeds, UK, 2001.

[5] Niels Fitzer, Angelika Kuligk, and Ronald Redmer. Full-band Monte Carlo simulations of high-field electron transport in gaas and zns. *Physical Review B*, 67, 2003.

[6] Paul Harrison. *Quantum Wells, Wires and Dots, Second Edition. Theoretical and Computational Physics of Semiconductor Nanostructures*. John Wiley & Sons Ltd., 2005.

[7] Mark Lundstrom. *Fundamentals of Carrier Transport*. Addison-Wesley Publishing Company, 1990.

List of author's publications

[TELECOMDAY] R. Reeder. Numerical solution of 1D Schrödinger equation for the example of double quantum wells. *Paper presented for the conference of International Telecommunication Day in Tallinn University of Technology (May 13, 2005, Tallinn, Estonia), "Raadiotehnika 2005", pp. 138-148.*

[BEC] R. Reeder, A. Udal, E. Velmre, and P. Harrison. Numerical investigation of digitised parabolic quantum wells for terahertz AlGaAs/GaAs structures. *Proc. of the 10th Biennial Baltic Electronic Conference BEC2006 (October 2-4, 2006, Tallinn, Estonia), pp. 51-54.* // Available through IEEE Xplore.

[ESTSCIPROC] A. Udal, R. Reeder, E. Velmre, and P. Harrison. Comparison of methods for solving the Schrödinger equation for multiquantum well heterostructure applications. *Proc. Estonian Acad. Sci. Eng.,* Volume 12, Number 3-2, *pp 246-261*, September 2006.

[JAP] R. Reeder, Z. Ikonić P. Harrison, A. Udal, and E. Velmre. Laterally pumped GaAs/AlGaAs quantum wells as sources of broadband THz radiation. *Manuscript submitted for the Journal of Applied Physics, 8 pages,* March 2007.

[ITQW07] R. Reeder, Z. Ikonić P. Harrison, A. Udal, and E. Velmre. Efficiency Estimation for a Broadband 7 THz Radiation Source with GaAs/AlGaAs Parabolic Quantum Wells. *Abstract for the Conference on Intersubband Transitions in Quantum Wells (September 9-14, 2007, Ambleside, Cumbria, U.K.), 2 pages.*

Copies of publications